High-Order Solution Scheme for Transport in Low-D Devices

F. Buscemi,[1] E. Piccinini, R. Brunetti,[1] M. Rudan
"E. De Castro" Advanced Research Center on Electronic Systems (ARCES) and Department DEI
University of Bologna, Viale Risorgimento 2, I-40136 Bologna, Italy — mrudan@arces.unibo.it
[1]Department of Physics, Informatics, and Mathematics
University of Modena and Reggio Emilia, Via Campi 213/A, I-41125, Modena, Italy

Abstract

The numerical approach to quantum transport in nanowires and nanotubes in the ballistic regime requires an accurate numerical solution of the coupled Schrödinger and Poisson equations. Here the feasibility of a 5th-order method is proved for the longitudinal part of the wave equation. The effectiveness of the method is demonstrated on a ballistic device.

Introduction

In the full-quantum analysis of ballistic transport in cylindrical-nanowire (CNW) and carbon-nanotube (CNT) devices (a sketch of the former is shown in Fig. 1), the problem is often solved by decoupling the Schrödinger equation along the radial (r) and longitudinal (z) coordinate [1]. After discretizing the latter from the source ($z = 0$) to the

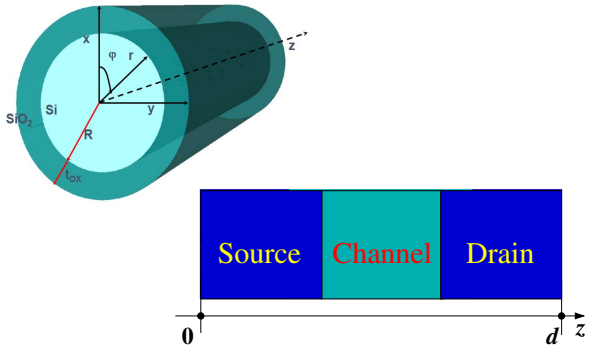

Fig. 1. A silicon, cylindrical nanowire (left, above); sketch of the simulated device (right, below). The channel is 8 nm long, both source and drain regions are 8.5 nm long.

drain ($z = d$) boundary, the Schrödinger equation is solved over the transverse section at each grid node z_i. Being this a closed-boundary problem, it yields a set of eigenvalues that provide the ground energies of the subbands for the longitudinal problem. The latter is then tackled by solving the longitudinal Schrödinger equation with open boundary conditions ("quantum-transmitting boundary method", QTBM), using the parabolic-band approximation. In this part of the solution the total energy E of the electron may take any value within each subband. For the electrons that are injected from the source (drain) into the channel the weight of each E is prescribed by the Fermi statistics $f(E)$ and the density of states $g(E)$ of the source (drain) lead.

As the ground energies are obtained from the solution of the Poisson equation, the problem entails the coupled solution of the Schrödinger-Poisson system. The transversal solution has two quantization indices (μ_1 and μ_2) and is quite expensive in itself. The longitudinal solution is less expensive, but must be repeated for all pairs μ_1, μ_2, each subband, and all values of E, that is, a huge number of times. For this reason it is convenient to reduce the number of grid nodes in the z direction. This, however, lowers the accuracy of the longitudinal solution and degrades the calculation of the wave function $w(z, E)$ and transmission coefficient $T(E)$. For this reason, numerical schemes of an accuracy higher than that of the standard Box-Integration-Method (BIM) are useful in this context. An efficient computational scheme, based on the *Numerov Process* (NP) [2], is illustrated in this paper and tested on a model problem; while its computational cost is the same as in BIM, its error is of the sixth order in the grid spacing η (specifically, the lowest-order term that is discarded is proportional to η^6).

Model

Following the reasoning outlined in the Introduction, the analysis here is limited to the longitudinal part of the problem. It is assumed that the solution of the lateral part, including the influence of the bias applied to the device gate, has preliminarily been obtained. As a consequence, the model problem for the longitudinal coordinate z is made of the time-independent Schrödinger equation for a particle of effective mass m, the Poisson equation, and the integral relation for the electron concentration. The first two equations read, respectively,

$$-\frac{\hbar^2}{2\,m}\,w'' - e\,\varphi\,w = E\,w\,, \qquad (1)$$

with φ the electric potential and e the elementary charge,

$$\varphi'' = \frac{e}{\varepsilon}\,(n_S + n_D - N)\,, \qquad (2)$$

with $n_{S(D)}$ the concentration of the electrons injected by the source (drain), and $N(z)$ the dopant concentration, here assumed of the donor type. The electron concentrations are given by [1]

$$n_{S(D)}(z) = \int_{E_{S(D)}}^{\infty} g_{S(D)}\,f_{S(D)}\,|w_{S(D)}|^2\,\mathrm{d}E\,, \qquad (3)$$

where suffix S (D) again refers to the source (drain) and $E_{S(D)}$ indicates the bottom of the conduction band at source (drain).

978-1-4799-5288-5/14/$31.00 © 2014 IEEE

The Numerov process provides a higher-order interpolation among three consecutive grid nodes (see Appendix). Despite the fact that the method was originally devised to solve the Schrödinger equation, a difficulty must be mentioned, that could spoil its application to open integrations like that of the present case: in fact, the first derivative w' at the left or right boundary, also necessary to start the open integration, must possess the same accuracy. However, the difficulty can be overcome; the details are given in [3], where boundary conditions having the same order of accuracy as the interpolation scheme are worked out.

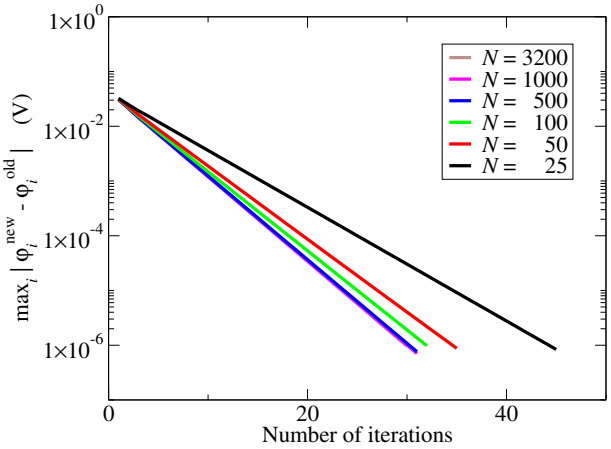

Fig. 2. Number of iterations necessary to reach convergence in the equilibrium condition. The legend indicates the number of gridpoints for each simulation.

The boundary conditions for the Poisson equation do not suffer the problem because the device is voltage driven: as a consequence, this equation yields a boundary-value problem. Moreover, the lack of the zeroth-order derivative in the Poisson equation provides a simpler form of the Numerov interpolation; in conclusion, letting $q(z) = 2\,m\,[E + e\,\varphi(z)]/\hbar^2$ and $\gamma = \eta^2/12$, the discretized form of (1) reads

$$s_{i+1}\,w_{i+1} + s_{i-1}\,w_{i-1} = 2\,(1 - 5\,\gamma\,q_i)\,w_i\,, \qquad (4)$$

where the suffix indicates the nodal value, and $s_j = 1 + \gamma\,q_j$. Eq. (4) is solved by a forward substitution, given $w_0 = w_{z=0}$ and w_1; the latter value is extracted from the boundary conditions w_0, $(\mathrm{d}w/\mathrm{d}z)_{z=0}$ [3]. In turn, letting $c = 2\,m\,e^2\,(n_S + n_D - N)/(\hbar^2\,\varepsilon)$, the discretized form of (2) reads

$$q_{i-1} - 2\,q_i + q_{i+1} = \gamma\,(c_{i-1} + 10\,c_i + c_{i+1})\,. \qquad (5)$$

The wave function w in (1) is defined apart from a multiplicative constant, whose value is determined as shown in the following. One notes that the density of states in (3) is one dimensional, namely, its units are (J cm)$^{-1}$; as a consequence, those of w are cm^{-1}. As shown below, w in the leads is proportional to a plane wave, so that its units are embedded in the multiplicative constant mentioned above. The value of the latter is obtained from a normalization condition imposing that the device is globally neutral at equilibrium. From the espression of charge density given by the right hand side of (2), the normalization condition is found to be

$$\int_0^s (n_S + n_D)\,\mathrm{d}z = \int_0^s N\,\mathrm{d}z\,, \qquad (6)$$

with $n_{S(D)}(z)$ given by (3).

Fundamental Solutions

Considering the two leads connected to the source and drain contacts, the potential energy $V(z) = -e\,\varphi$ is prescribed as $V = V_S = $ const. for $z \le 0$ and $V = V_D = $ const. for $0 < d \le z$. As $E > V_S, V_D$, the total energy is not quantized and all values of E larger than V_S and V_D are allowed. The solution of (1) in the left and right lead is a combination of plane waves

$$w_S = a_1\,\exp(j\,k_S\,z) + a_2\,\exp(-j\,k_S\,z)\,, \qquad (7)$$

$$w_D = a_5\,\exp(j\,k_D\,z) + a_6\,\exp(-j\,k_D\,z)\,, \qquad (8)$$

$$k_{S(D)} = \frac{1}{\hbar}\sqrt{2\,m\,(E - E_{S(D)} - V_{S(D)})}\,, \qquad (9)$$

with a_i undetermined coefficients. It is $a_6 = 0$ ($a_1 = 0$) when the particle is launched from the left (right). In the interval $0 \le z \le d$ the general solution of (1) is

$$w = a_3\,u(z) + a_4\,v(z)\,, \qquad (10)$$

where u, v are the two fundamental solutions of (1) in $0 \le z \le d$, fulfilling the boundary conditions $u(0) = 1$, $u'(0) = 0$, $v(0) = 0$, $v'(0) = 1$. Expression (10) of w is convenient because it allows one to solve (1) for u and v, using the interpolation scheme (4), without considering the matching relations at the boundaries. The relations among coefficients are determined afterwards, using the fundamental solutions thus obtained. For instance, for an injection from the source the continuity of the wave function and its derivative at $z = 0$ and $z = d$ yields

$$\left(\frac{a_2}{a_1}\right)_S = -\frac{u'_d + j\,k_S\,v'_d - j\,k_D\,(u_d + j\,k_S\,v_d)}{u'_d - j\,k_S\,v'_d - j\,k_D\,(u_d - j\,k_S\,v_d)}\,. \qquad (11)$$

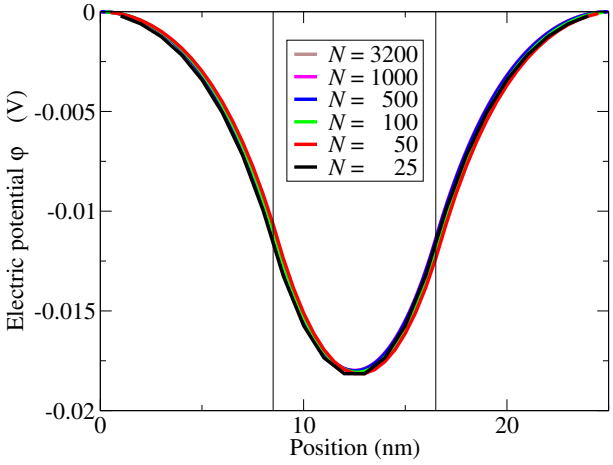

Fig. 3. Profile of the electric potential φ inside the device, at equilibrium. The two vertical lines mark the ends of the channel.

In turn, the expression of w_S to be used in (3) is

$$w_S = a_1 \left[\left(1 + \frac{a_2}{a_1} \right)_S u + j\, k_S \left(1 - \frac{a_2}{a_1} \right)_S v \right] , \quad (12)$$

with a_1 still arbitrary. The injection from the drain is treated in a similar manner, to yield

$$\left(\frac{a_2}{a_6} \right)_D = - \frac{2\, j\, k_D \, \exp(-j\, k_D\, d)}{u'_d - j\, k_S\, v'_d - j\, k_D\, (u_d - j\, k_S\, v_d)} , \quad (13)$$

$$w_D = a_6 \left(\frac{a_2}{a_6} \right)_D (u_d - j\, k_S\, v_d) , \quad (14)$$

with a_6 arbitrary. Finally, the normalization constant is

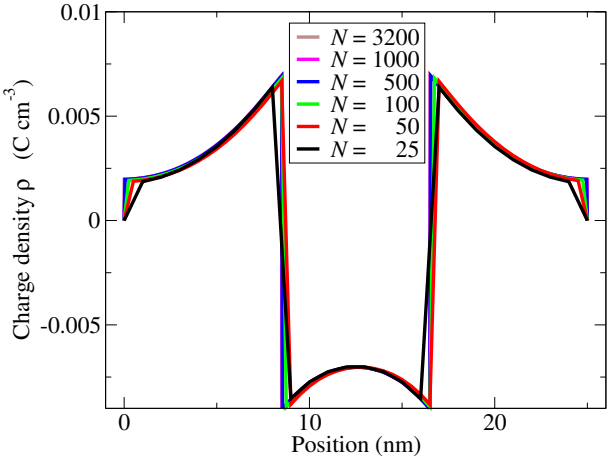

Fig. 4. Profile of the charge density ϱ inside the device, at equilibrium.

worked out by letting $a_6 = a_1$ and inserting (12,14) into (3) and then into (6).

Results and Discussion

The figures refer to a 25 nm-long device whose channel is lightly doped ($N = 10^{14}$ cm^{-3}) and has a length of 8 nm (Fig. 1). The source and drain regions are 8.5 nm long, with a dopant concentration equal to $N = 10^{17}$ cm^{-3}. The lateral size is small enough to make the Fermi statistics significant for the first subband only; the data for the one-dimensional density of states of the latter, $g \propto E^{-1/2}$, are taken from [1]. The zero of the electric potential is made to coincide with the bottom of the conduction band at the left boundary; the bottom of the conduction band on the right is set to $V_D = -q\, \varphi_D$, where the applied bias φ_D is made to range from 0 to 1 V. Charge neutrality is assumed at the contacts.

The analysis has been carried out starting with a large number of grid nodes ($M = 3.200$) and progressively decreasing it to $M = 75$. The tentative solution used to start the iterative procedure was $\varphi'' = 0$ in all cases. The convergence criterion has been set to

$$\max_i |\varphi_i^{\rm new} - \varphi_i^{\rm old}| \leq 1 \;\; \mu{\rm V} , \quad (15)$$

with i the nodal index.

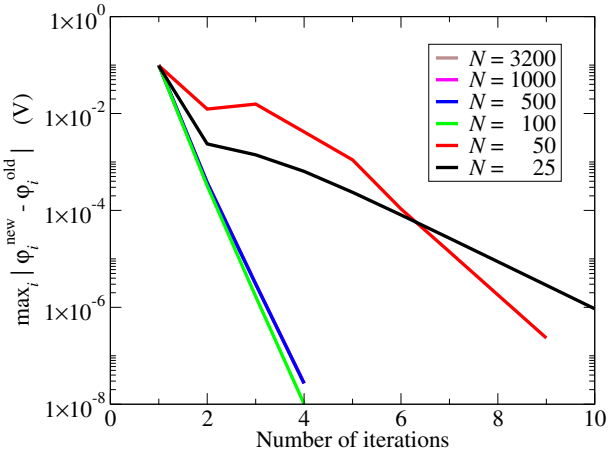

Fig. 5. The same as in Fig. 2, with an applied bias $\varphi_D = 1$ V.

The number of iterations necessary to fulfill criterion (15) in the equilibrium case ($\varphi_D = 0$) is shown in Fig. 2, using the number of nodes as parameter. The convergence rate turns out to be about the same for M ranging from 3.200 to 50, whereas it starts increasing when the number of grid nodes becomes smaller than 50. The electric potential φ obtained from a self-consistent solution of (1), (2), and (3), still in the equilibrium condition, is shown in Fig. 3, with the vertical lines marking the channel ends. Although the coarseness of the discretization is clearly visible in the $M = 25$ case, the curves essentially overlap each other. The charge density corresponding to the electric potential of Fig. 3 is shown in Fig. 4; as this function is obtained from (3), its calculation is the most delicate part of the solution process. The sharp variations in the charge density at the ends of the channel correspond to changes in the slope of the curves of Fig. 3 at the same positions; such changes are not easily seen due to the figure's scale.

The number of iterations necessary to fulfill criterion (15) at the largest applied voltage ($\varphi_D = 1$ V) is shown in Fig. 5, still using the number of nodes as parameter. The number of iterations is smaller than at equilibrium (compare with Fig. 2); this is due to the fact that the charge density within the device becomes smoother as the applied bias increases, at least in the bias range considered here. The convergence rate turns out to be about the same for M ranging from 3.200 to 100; it starts increasing when the number of grid nodes becomes smaller than 100, but remains significantly below the equilibrium value.

The charge density corresponding to $\varphi_D = 1$ V is shown in Fig. 6. The results show that the method exhibits the same behavior down to $M = 100$ at least, whereas some spurious oscillations become apparent when the number of grid nodes is lower (e.g., the curves corresponding to $M = 50$ and $M = 25$). This is to be expected, because the wave function in the source and drain regions is of the oscillatory type ($w \simeq \exp(\pm j\, k\, z)$), so that the discretization is effective if the period $Z = 2\,\pi/k$ of w

fulfills the constraint $Z \gg d/M$, equivalent to

$$E - E_{S(D)} \ll \frac{(2\,\pi\,\hbar)^2}{2\,m\,d^2}\,M^2\,, \qquad (16)$$

in the energy range where the Fermi statistics differs significantly from zero (compare with the integral in (3)). If one takes $m = 0.5\ m_0$, with m_0 the free electron's mass, and uses $d = 25$ nm, the fraction at the right hand side of (16) is about 4.8 meV. The constraint (16) is not fulfilled any more when M becomes low.

Finally, Fig. 7 shows the charge density at different biases, with φ_D ranging from 0 to 1 V, and $M = 3200$. As the bias departs from the equilibrium value, the charge distribution undergoes a sudden variation due to the ballistic regime. In conclusion, an effective application of a higher-order solution method has been implemented and tested. It has been applied to self-consistently solve the longitudinal part of the coupled Schrödinger-Poisson system, typical of ballistic devices; the problem is particularly severe because it entails an open integration where the number of grid nodes must be kept as low as possible to limit the numerical burden of the transversal part of the equations.

References

[1] E. Gnani, A. Marchi, S. Reggiani, M. Rudan, and G. Baccarani, "Comparison of device performance and scaling properties of cylindrical-nanowire (CNW) and carbon-nanotube (CNT) transistors", in Proc. SISPAD-2006. Monterey, CA: IEEE pp. 23–26 (2006).

[2] B. Numerov, Publ. Obs. Central Astrophys. 2, 188 (1933), cited in P. C. Chow, AJP 40, 730 (1972).

[3] F. Buscemi, M. Rudan, E. Piccinini, R. Brunetti, "A 5th-Order Method for 1D-Device Solution", Proc. IWCE, Paris (2014).

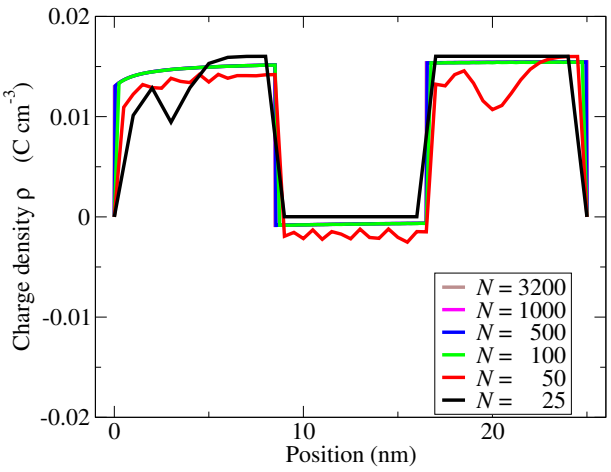

Fig. 6. The same as in Fig. 4, with an applied bias $\varphi_D = 1$ V.

Appendix

The Numerov Process is derived as follows. Consider three consecutive, equally-spaced nodes of the grid, such that $z_{i-1} < z_i < z_{i+1}$, and Taylor expand a function f from the central node i to the $(i+1)$th one,

$$f_{i+1} = f_i + \eta\,f_i' + \frac{\eta^2}{2}\,f_i'' + \dots\,, \qquad (17)$$

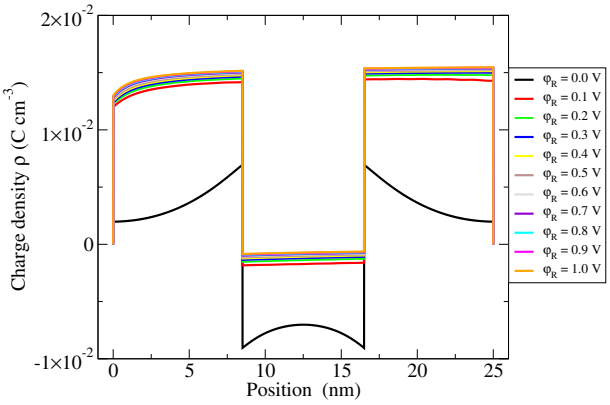

Fig. 7. Charge density ϱ at different biases, with φ_D ranging from 0 to 1 V.

where the superscripts indicate derivatives and η is the grid spacing. A similar expansion from i to $i-1$ has the same even powers as (17), whereas the odd powers have the opposite sign. When the two expansions are summed up, the odd powers cancel each other; if the result is truncated by leaving out the sixth order, one finds

$$f_{i+1} + f_{i-1} \simeq 2\,f_i + \eta^2\,f_i'' + \frac{\eta^4}{12}\,f_i''''\,. \qquad (18)$$

As (18) holds for any function, it holds for f'' as well. This yields, again leaving out the sixth order,

$$f_{i+1}'' + f_{i-1}'' \simeq 2\,f_i'' + \eta^2\,f_i''''\,. \qquad (19)$$

Elimination of f_i'''' between (18) and (19) provides a relation of the form

$$f_{i+1} + f_{i-1} \simeq 2\,f_i + \frac{\eta^2}{12}\left(f_{i+1}'' + f_{i-1}'' + 10\,f_i''\right)\,. \qquad (20)$$

If f is the solution of a second-order differential equation like (1), one has $f = w$, $w'' = -q\,w$. Replacing the second derivative into (20) yields (4). If, instead, f is the solution of a second-order differential equation like $q'' = c$, with c a given function (compare with (2)), letting $f = q$ and replacing the second derivative in (20) yields (5).

The calculations leading to (20) imply that the grid is uniform. This is not too severe a constraint for the problem considered in this paper. On the other hand, if necessary, a regional approach is also feasible, where the domain is parted into subdomains such that the grid spacing is uniform within each subdomain, but different from one subdomain to another. The connection between two subdomains is achieved using the same method depicted in [3], that preserves the accuracy of the numerical scheme.